IEEE Access
Multidisciplinary | Rapid Review | Open Access Journal

Received July 25, 2020, accepted August 15, 2020, date of publication August 31, 2020, date of current version September 14, 2020.

Digital Object Identifier 10.1109/ACCESS.2020.3020325

Spectral Index Fusion for Salinized Soil Salinity Inversion Using Sentinel-2A and UAV Images in a Coastal Area

YING MA, HONGYAN CHEN, GENGXING ZHAO, ZHUORAN WANG, AND DANYANG WANG

National Engineering Laboratory for Efficient Utilization of Soil and Fertilizer Resources, College of Resources and Environment, Shandong Agricultural University, Tai'an 271000, China

Corresponding author: Hongyan Chen (chenhy@sdau.edu.cn)

This work was supported in part by the Natural Science Foundation of Shandong Province, China, under Grant ZR2019MD039, in part by the National Natural Science Foundation of China under Grant 41877003 and Grant 41671346, and in part by the Funds of Shandong Double Tops Program under Grant SYL2017XTTD02.

ABSTRACT The accurate and rapid inversion of soil salinity in regions based on the fusion of multisource remote sensing is not only practical for the treatment and utilization of saline soil but also the main trend in the development of quantitative soil salinization remote sensing. In this paper, the use of a numerical regression method to fuse spectral indexes based on high-spatial-resolution unmanned aerial vehicle (UAV) images and low-spatial-resolution satellite images was proposed to deeply assess the internal relationships between different types of remote sensing data. An inversion model of soil salt content (SSC) was constructed based on high-spatial-resolution UAV images, and the spectral indexes involved in the fusion were selected from the model. Then, a quadratic polynomial fusion function describing the relationship between the spectral indexes based on the two images was established to correct the spectral indexes based on the low-spatial-resolution satellite image (from Sentinel-2A). Then, scenario 1 (the best model based on Sentinel-2A used for the unfused Sentinel-2A spectral index), scenario 2 (the best inversion model based on UAV used for the unfused Sentinel-2A-based spectral index), and scenario 3 (the best inversion model based on UAV used for the fused Sentinel-2A-based spectral index) were compared and analyzed, and the SSC distribution map was obtained through scenario 3. The results indicate that the scenario 3 had highest accuracy, with the calibration R^2 improving by 0.078-0.111, the root mean square error (RMSE) decreasing by 0.338-1.048, the validation R^2 improving by 0.019-0.079, the RMSE decreasing by 0.517-1.030, and the ratio of performance to deviation (RPD) improving by 0.185-0.423. Therefore, this method can improve the accuracy of SSC remote sensing inversion, which is conducive to the accurate and rapid monitoring of SSC.

INDEX TERMS Soil salinization, spectral index fusion, numerical regression, unmanned aerial vehicle.

I. INTRODUCTION

Soil salinization is the main land degradation problem in most arid and semiarid agricultural areas in the world, seriously restricting the development of regional ecological agriculture [1]–[5]. Therefore, it is very important to quickly and accurately obtain information on the spatial distribution of soil salt content (SSC) for the prevention and improvement of saline soil and the enhancement of ecological agriculture [6], [7]. Remote sensing has become an effective way to quantitatively extract salinization information [8]. Satellite imaging has become the mainstream agricultural remote sensing method because of its advantages in acquiring soil information over a large area [9]–[13]. However, due to its discontinuity across space and time, low resolution, and vulnerability to weather conditions, it lacks timeliness and accuracy. In recent years, unmanned aerial vehicle (UAV), as a new remote sensing platform, has been used to acquire images in a research area through using a variety of sensors, and then constructs a model to realize the inversion of target parameters in a small area [14]–[18]. This technique has the advantages of low cost and ease of construction. UAV technology has been of interest. However, due to limitation of flight time and altitude, it is difficult to achieve large-scale quantitative inversion. Thus, it can be seen that it is difficult for single sensor to meet the information extraction requirements for SSC with high

The associate editor coordinating the review of this manuscript and approving it for publication was Peng Liu.

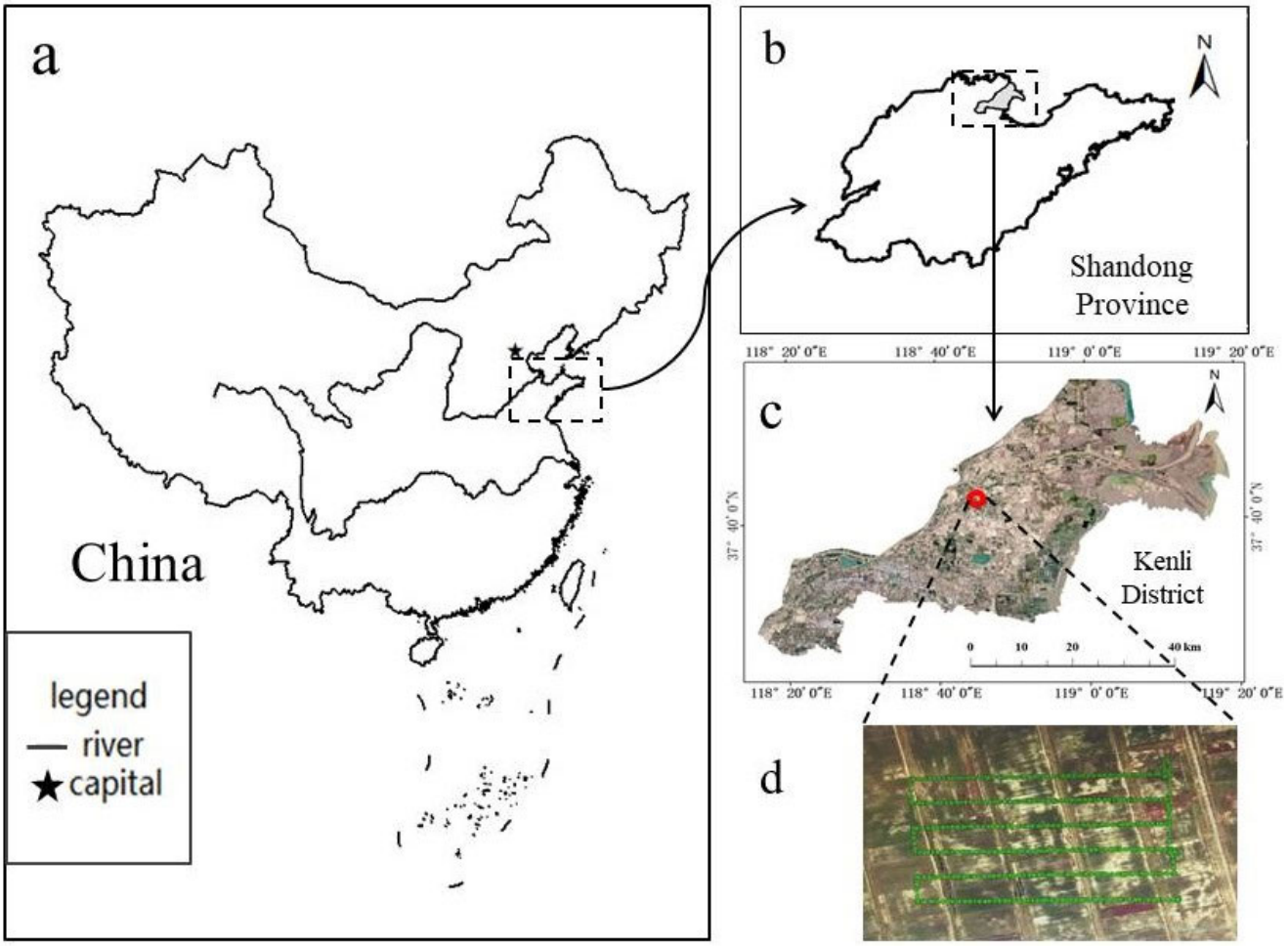

FIGURE 1. The study area and the test area ((a) China, (b) Shandong Province, (c) Kenli district and (d) The test area and UAV flight route).

precision, across a large area and with a fast rate. Research on SSC inversion based on satellites, UAV and other multisource remote sensing fusion applications has become a hot topic [19], [20].

The fusion of multisource remote sensing can be divided into three levels: spectral data fusion (pixel level), spectral model fusion (decision level) and spectral index fusion (feature level) [21]–[25].

Spectral data fusion involves the fusion of the original observation or preprocessed data from sensors to generate new data. Its main purpose is to improve the data quality. For example, Ilyas *et al.* [26] integrated Phased Array Type L-band SAR (PLSAR) and Landsat Enhanced Thematic Mapper Plus (ETM+) data to monitor the SSC of the Kriya River basin in northwest China. However, fusion based on spectral data requires the calculation of each pixel, which involves a large amount of data processing. Moreover, it is difficult to verify the consistency of the features contained in the original data from various sensors, and thus image fusion based on pixels has certain blindness. In spectral model fusion, quantitative analysis models are first established based on different remote sensing data and then fused to correct and identify the models with the lowest accuracy. For example, Adak Klimi *et al.* [27] used the SSC estimation model based on measured hyperspectral data to correct the SSC inversion model based on advanced spaceborne thermal emission and reflection radiometer (ASTER) multispectral images, which improved the accuracy of soil salinization monitoring at the regional scale. However, in this kind of fusion, the corresponding models first need to be established based on the different types of original data used to obtain the respective decision results, and the fusion has high requirements for pretreatment and feature extraction. Moreover, the fusion results depend on the advantages and disadvantages of the established models to some extent, and the accuracy is relatively poor.

Between spectral data fusion and spectral model fusion, spectral index fusion extracts the spectral indexes from the data from different sensors separately and then fuses the spectral indexes to obtain the new spectral indexes. It has the advantages of a fast processing speed and few calculations, which has caused it to become the main fusion method at present and widely used. For example, He *et al.* [28] fused the spectral indexes from remote sensing data on the

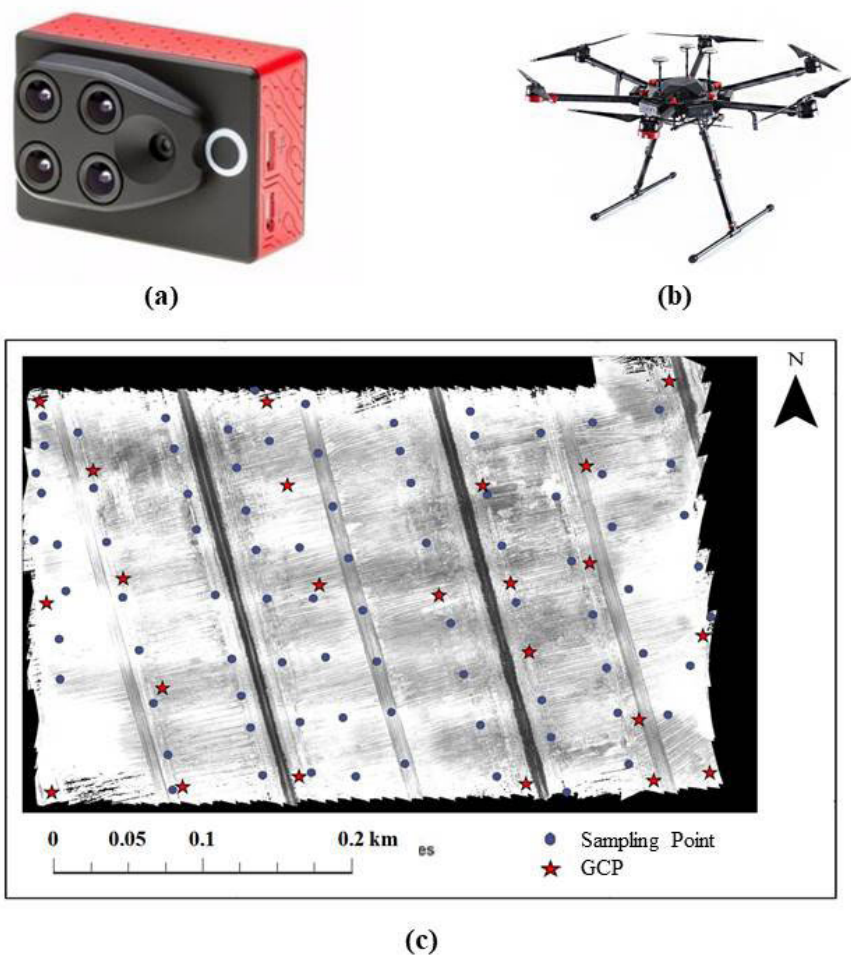

FIGURE 2. UAV image acquisition ((a) Sequoia agricultural multispectral camera, (b) Matrice 600 Pro hexacopter, (c) false-color composite image and sampling point distribution in the test area).

fine particulate matter (PM2.5) concentration, land surface temperature (LST) and vegetation cover (VC) and built a comprehensive evaluation index to study the environmental degradation in urban areas of China. However, most of the existing research based on multisource remote sensing fusion has been performed by building a simple parameter relation of the spectral indexes from different sensors. For example, Li *et al.* [29] used the two methods of central wavelength reflectance and average band reflectance to fit ground hyperspectra and Landsat 8 data, revised the satellite imagery by calculating the ratio of the mean spectral indexes from the ground hyperspectra and Landsat 8 data, and then conducted remote sensing inversion of the soil water content in the study area. This kind of construction form is relatively simple and without in-depth mining of the internal relationship between satellite and UAV data, but the inversion accuracy still needs to be improved. Therefore, whether there is a good relationship between satellite and UAV multispectral imaging and how to improve the fusion method to improve the accuracy of SSC inversion need to be further explored.

The purpose of this paper is to combine the advantages of the high spatial resolution of UAV multispectral imaging and the large scale of Sentinel-2A satellite imaging (Sentinel-2A) and explore a numerical regression method to fuse spectral indexes to conduct accurate SSC inversion for Kenli district, Yellow River Delta, China, where salinization is severe. In contrast to previous studies, in this study, we first constructed the SSC inversion model based on UAV and selected the spectral indexes from the model for fusion. On this basis, the feasibility of data fusion was judged by fitting analysis between the optimized spectral indexes based on UAV and Sentinel-2A. Then, a fusion function of quadratic polynomials between the Sentinel-2A-based and UAV-based spectral indexes was established with the numerical regression method, and the Sentinel-2A-based spectral indexes were corrected. Finally, the SSC inversion model based on UAV was applied to the corrected Sentinel-2A data to obtain the inversion map of SSC in the study area.

This paper is organized as follows. Section II describes the study area and datasets. In Section III, the specific process of fusing data on the basis of numerical regression is described in detail. Experimental results are shown in Section IV. Section V and Section VI present the discussion and conclusions, respectively.

TABLE 1. Corresponding relationships between Sentinel-2A and UAV data.

Name	Sequoia (UAV)				Sentinel-2A			
	Band	Central wavelength (nm)	Bandwidth (nm)	Resolution (m)	Band	Central wavelength (nm)	Bandwidth (nm)	Resolution (m)
G	Green	550	40	0.05	B_3-Green	560	45	10
R	Red	660	40	0.05	B_4-Red	665	38	10
REG	Red Edge	735	10	0.05	B_6-Vegetation Red Edge	740	18	20
NIR	Near IR	790	40	0.05	B_7-Vegetation Red Edge	783	28	20

TABLE 2. Statistical characteristics of the soil samples.

Statistical indicator	Numerical value ($g \cdot kg^{-1}$)
Maximum value	23.400
Minimum value	0.243
Average value	7.136
Standard deviation	5.105
Coefficient of variation	0.716

II. STUDY AREA AND DATASET

A. OVERVIEW OF THE STUDY AREA

The study area is located in Kenli district, Yellow River Delta, the west bank of Laizhou Bay and the south bank of Bohai Bay, China (Fig. 1). The study area has a temperate monsoon climate, and its terrain is mainly plain with slight slopes from the southwest to the northeast [30]. The study area is vast, with a total area of 2331 square kilometers, and the Yellow River carries sand to generate thousands of hectares of land every year, which provides rich land reserve resources for China.

However, the soil in the study area is developed on the alluvial deposits of the Yellow River, and sandy loam is dominant. Due to the infiltration of water from the Yellow River, the top support and immersion of the sea water, and the sea water flowing back to the land, the secondary salinization of the soil is relatively severe, which results in a lack of seedlings, the death of crops, and low farmland yield, affecting the income level of villagers, hindering the development of the regional social economy, degenerating the ecological environment, and seriously threatening the local ecological balance.

B. DATA ACQUISITION AND PREPROCESSING

1) FIELD MEASUREMENT OF SOIL SALINITY

In spring, the precipitation in the study area is low and the evaporation is high, causing the salt content of the soil surface to also be high, making it the best time to obtain SSC information. Therefore, the sampling date was April 26, 2018.

Based on natural factors such as topography, hydrology, climate, the saline soil area south of the central kindergarten of Xisong village, Huanghekou town, Kenli district, was selected as the test area (118° 40' 50''-118° 43' 00'' E, 37° 39' 29''-37° 39' 40'' N), covering a total area of 24.675 hectares. During sampling, the surface of the test area was continuously exposed, lacking vegetation coverage. In the test area, 85 sampling points and 22 ground control points (GCPs) were established, both the samples and GCPs were evenly distributed. The salt score of the soil surface (10 cm) was measured with an EC110 portable salinity meter (Spectrum Technologies, Inc., USA), the coordinates (longitude and latitude) of the sampling points were measured with a Trimble GEO 7X centimeter handheld differential GPS (Trimble, Inc., Sunnyvale, California, USA), and the corresponding environmental information was recorded.

2) ACQUISITION AND PROCESSING OF UAV IMAGERY

At 11 a.m. on April 26, 2018, a Dajiang Matrice 600 Pro hexacopter (SZ DJI Technology Co., Ltd, Shenzhen, Guangdong Province, China) with a Sequoia agricultural multispectral camera was used to obtain UAV imagery (Fig. 1d). The camera captures four bands: green (wavelength 550 nm, bandwidth 40 nm), red (wavelength 660 nm, bandwidth 40 nm), red edge (wavelength 735 nm, bandwidth 10 nm) and near infrared (wavelength 790 nm, bandwidth 40 nm). According to the actual geographical environment factors, the UAV flight height (52 m), flight speed (5 $m \cdot s^{-1}$), flight path, continuous shooting time interval (1.5 s), course and side direction overlap (60%) and other parameters were determined before takeoff, and radiation correction of the UAV whiteboard was carried out. Then, Pix4Dmapper software (Pix4D S.A. Route de Renens 241008, Prilly, Switzerland) was used to achieve extrinsic radiation calibration, spectral calibration and the image mosaic. The software ENVI 5.3 (Exelis Visual Information Solutions, Inc., USA) was used for geometric correction and the geographical registration of

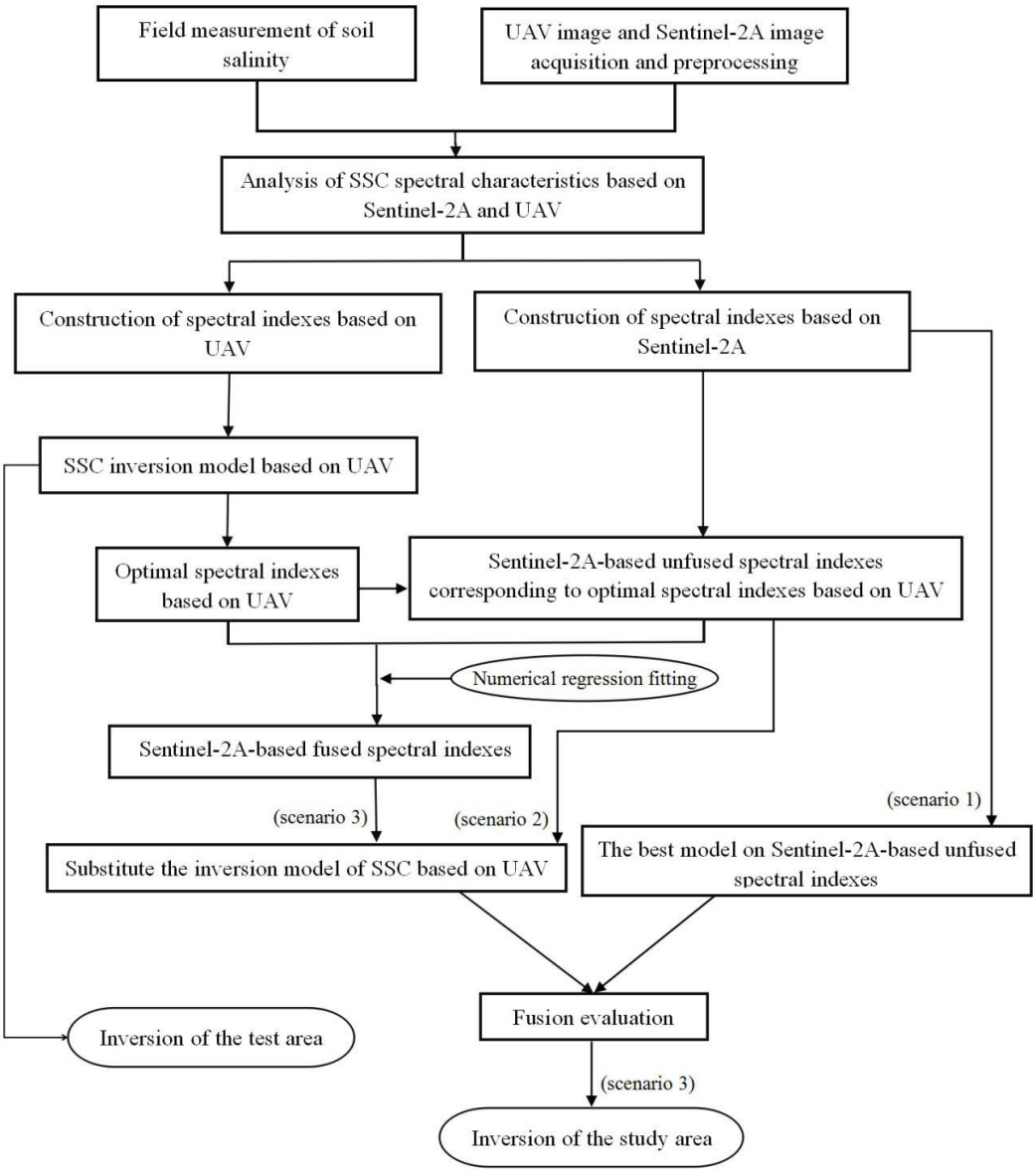

FIGURE 3. Technique flowchart.

ground control point data, and the accuracy of the selected control points was analyzed with a maximum accuracy error of a single point of 0.53 pixels, a minimum of 0.15 pixels, and a total average error of 0.39 pixels. Then, the image was resampled to 1 m. Finally, a false-color synthetic-band image (Fig. 2) was obtained with a resolution of 1 m.

3) ACQUISITION AND PROCESSING OF SENTINEL-2A IMAGERY

The Sentinel-2A products from the website of the European Space Agency (ESA, http://www.esa.int/) were used as satellite remote sensing image data. First, on April 27, 2018, the Sentinel-2 L1C image data (https://scihub.copernicus.eu/) covering the study area were downloaded, representing the atmospheric apparent reflectance product after geometric precision correction [31]. Using the Sentinel Application Platform (SNAP) software provided by the ESA, atmospheric correction and radiometric calibration were applied to the data, the Sentinel-2A data were resampled to 1 m such that the pixel sizes were the same as in the UAV image, and finally the data were exported in ENVI format. Then, the data were imported into ENVI 5.3. The bands (B3-Green, B4-Red, B6-Vegetation Red Edge, and B7-Vegetation Red Edge) were relatively consistent with the band range of the Sequoia multispectral camera and were selected for image splicing, band synthesis, image clipping and other preprocessing procedures (Table 1).

On the basis of the actual situation in the study area, the normalized difference vegetation index (NDVI) was used to generate a mask for the area with a NDVI less than 0 to remove the water areas in the image [32], and then the linear binary model pixel decomposition method was used to remove the impact of vegetation [33]. Finally, the processed image was used as the Sentinel-2A image for the study area.

TABLE 3. SSC correlation between UAV and Sentinel-2A bands.

Band name	Correlation coefficient	
	UAV	Sentinel-2A
G	-0.645*	-0.495*
R	-0.649*	-0.457*
REG	-0.595*	-0.473*
NIR	-0.642*	-0.446*

Note: * significant correlation at the 0.05 level

III. METHODS

A. ANALYSIS OF SSC SPECTRAL CHARACTERISTICS BASED ON SENTINEL-2A AND UAV

The spectral reflectance at the sampling points based on UAV and Sentinel-2A were extracted with ArcGIS 10.2 software according to the GPS coordinates, and the correlation between the reflectance and salt value of the sampling points was analyzed (with the correlation coefficient expressed as R). Then, the SSC response bands based on Sentinel-2A and UAV were compared and analyzed.

B. CONSTRUCTION AND OPTIMIZATION OF THE SSC INVERSION MODEL BASED ON UAV

Based on the UAV-based SSC response bands, simple combination operations, such as B_i-B_j, B_i/B_j, and $(B_i-B_j)/(B_i+B_j)$, were performed among multiple bands to construct the spectral indexes [34]–[38], and the correlations between the spectral indexes and SSC were analyzed. In the formulas, B_i and B_j represent the band name.

Eighty-five samples were divided into two groups according to a ratio of two to one; 56 were used for calibration, and the other 29 were used for validation. The calibration and validation datasets conformed to the assumption of variance homogeneity [39]. Taking the salt value of the calibration sample as the dependent variable and the spectral indexes as the independent variables, the multivariate stepwise linear regression method (MSLR) [40] was used to screen the SSC spectral parameters based on UAV and construct the inversion model. Then, the inversion model was validated with the validation samples. The performance of the SSC inversion models was evaluated according to the coefficient of determination (R^2), the root mean square error (RMSE), and the ratio of performance to deviation (RPD). A fitting graph between the estimated value and the measured value was drawn, and R^2 was used to evaluate the fitting effect. SPSS 20 (Statistical Product and Service Solutions) was used to build the model.

C. FUSION OF THE SSC SPECTRAL INDEX BASED ON SENTINEL-2A AND UAV

1) ANALYSIS OF THE RELATIONSHIP BETWEEN SENTINEL-2A-BASED AND UAV-BASED SPECTRAL INDEXES

According to the SSC optimization spectral indexes based on UAV, the corresponding spectral indexes based on the Sentinel-2A image were constructed. Fitting analysis of the spectral index homonymous pixels based on Sentinel-2A and UAV was carried out to explore the data consistency between the Sentinel-2A-based spectral indexes and UAV-based spectral indexes. The equation of fitting degree (R^2) is as follows [41]:

$$R^2 = 1 - \sum \left(y_{s,i} - y_{u.i}\right)^2 \Big/ \sum \left(y_{u,i} - \bar{y}_{u,i}\right)^2 \quad (1)$$

where $y_{u,i}$ is the value of a certain point on the specific spectral index based on the UAV image, $\bar{y}_{u,i}$ is the average value of the sample spectral index, and $y_{s,i}$ is the value of the homonymous point on the corresponding spectral index to be converted based on the Sentinel-2A image. $i = 1, 2, \cdots, n$

2) FUSION OF SENTINEL-2A-BASED AND UAV-BASED SPECTRAL INDEXES BY NUMERICAL REGRESSION

The numerical regression method is generally used to build the corresponding relationship between data by employing a polynomial function such that one set of data can approach another by fitting.

The quadratic polynomial fitting function of the optimized spectral indexes based on UAV and Sentinel-2A was established by the numerical regression method, and the conversion relationship between the same spectral index based on two different sensors was constructed. The fused Sentinel-2A-based spectral indexes were reconstructed using the fitting function. Then, the correlation between unfused and fused spectral indexes and SSC was compared. The regression fitting was in the form of a quadratic polynomial, as shown below [42]:

$$S_i' = a \times S_i^2 - b \times S_i + c \quad (2)$$

where a and b are spectral index conversion coefficients, c is the conversion residual, S_i is the unfused Sentinel-2A-based spectral index i, and S_i' is the fused Sentinel-2A-based spectral index i.

D. INVERSION AND ANALYSIS OF THE SSC SPATIAL DISTRIBUTION IN THE REGION

1) INVERSION AND ANALYSIS OF THE SSC SPATIAL DISTRIBUTION IN THE TEST AREA

Based on the best SSC inversion model, the Band Math tool in ENVI 5.3 software was used to compute the bands based on UAV. In ENVI Classic, the decision tree method was used to grade the different salt contents. For the classification of salt content, the coastal saline soil classification standard with chloride as the main soluble salt was

TABLE 4. Spectral index analysis based on UAV.

Spectral index	Formula	Correlation coefficient	Reference
Salinity index	$\sqrt{R \times G}$	-0.699*	D Abdelkader [33]
	$\sqrt{R^2 + G^2}$	-0.686*	
Green-red vegetation index	$(R - G)/(R + G)$	-0.193	C.J.Tucker [34]
Intensity index	$R + G$	-0.667*	HT Fourati [35]
	$R + NIR + G$	-0.670*	
New spectral index	$R \times G$	-0.625*	S. Zhang [36]
	R/G	0.009	
	$R - G$	-0.006	
	$G \times NIR$	-0.666*	
	$G \times NIR \times R$	-0.569*	
	$R \times NIR$	-0.597*	
	$R + NIR$	-0.674*	
	$R + NIR + REG$	-0.646*	
	$(REG - G)/(REG + G)$	0.266	
	$G + R + REG$	-0.695*	
	$REG - NIR$	0.649*	
	$REG - R$	0.652*	
	REG / R	0.314	
	$G + REG$	-0.632*	
	$G \times REG$	-0.644*	
	$R \times REG$	-0.651*	
	$R + REG$	-0.640*	
Red-edge spectral index	$(REG - R)/(REG + R)$	0.317*	J Wang [37]
	$\sqrt{R^2 + REG^2}$	-0.642*	
	$G^2 + REG^2$	-0.661*	
	$\sqrt{R \times REG}$	-0.637*	
	$\sqrt{REG \times G}$	-0.690*	
	$(REG - NIR)/(REG + NIR)$	-0.058	
	$G \times R \times REG$	-0.557*	
	$\sqrt{R^2 + REG^2 + G^2}$	-0.635*	
	$\sqrt{R \times REG \times G}$	-0.642*	
	$R + REG + NIR + R$	-0.664*	
	$R + NIR + REG$	-0.622*	

Note: * significant correlation at the 0.05 level

adopted: non-salinization (<2 g·kg^{-1}), mild salinization (2-4 g·kg^{-1}), moderate salinization (4-6 g·kg^{-1}), severe salinization (6-10 g·kg^{-1}) and solonchak (>10 g·kg^{-1}) [43]. Then, the SSC inversion map of the test area was obtained. To evaluate the modeling method, the samples were also divided into the five aforementioned soil salinity grades according to the ground truth data and are shown in the SSC inversion map.

2) INVERSION OF THE SSC SPATIAL DISTRIBUTION IN THE STUDY AREA

First, based on the Sentinel-2A-based response bands, the spectral indexes were constructed, and taking the salt value of the calibration sample as the dependent variable and the spectral indexes as the independent variable, the MSLR was used to construct the SSC inversion model based on Sentinel-2A. Then, the inversion accuracy of scenario 1 (the best model based on Sentinel-2A used for the unfused Sentinel-2A spectral index), scenario 2 (the best inversion model based on UAV used for the unfused Sentinel-2A-based spectral index), and scenario 3 (the best inversion model based on UAV used for the fused Sentinel-2A-based spectral index) was compared and analyzed. Finally, the effectiveness of spectral index fusion was verified, and the best scenario was applied to the Sentinel-2A image of the study area to perform the inversion of the SSC spatial distribution.

The technique flow of this study is shown in Fig. 3.

IV. EXPERIMENTAL RESULTS

A. DESCRIPTIVE STATISTICAL CHARACTERISTICS OF THE SSC OF THE SOIL SAMPLES

The statistical results of the SSCs of the samples show that the SSC in the test area is relatively high. According to the

TABLE 5. SSC model based on UAV by using MSLR.

Variable	Coefficient	Calibration		Validation		
		R^2	RMSE	R^2	RMSE	RPD
Constant	58.86					
G × NIR	166.92					
REG − NIR	87.46					
$\sqrt{REG \times G}$	-1273.27	0.68	3.07	0.71	2.98	2.01
G + R + REG	197.59					
$\sqrt{R \times G}$	505.55					
REG − R	479.90					

standard deviation and coefficient of variation, the SSCs are scattered.

B. SSC SPECTRAL CHARACTERISTICS BASED ON SENTINEL-2A AND UAV

The soil salinity and reflectivity of each band based on UAV are negatively correlated, R is in the range of −0.595 - −0.649, and the bands with high correlation are red, green and near red. The soil salinity and reflectance of each band based on Sentinel-2A are also negatively correlated, R is in the range of −0.446 - −0.495, and the bands with high correlation are green, red and red edge (Table 3). The correlation between the reflectivity based on the UAV image and SSC is better than that based on the Sentinel-2A image, and the band sensitive to the SSC based on the two images is relatively consistent, and thus it is feasible to fuse the two images. In addition, there is no significant difference between the bands based on Sentinel-2A and UAV, and each response band can participate in the construction of spectral indexes.

C. SSC INVERSION MODEL BASED ON UAV

1) CONSTRUCTED SPECTRAL INDEXES

According to the 33 constructed groups of UAV-based spectral indexes (Table 4), the R of the spectral indexes is significantly higher than that of the single characteristic band.

2) SSC INVERSION MODEL BASED ON UAV

According to the decision coefficients of the calibration set and the validation set (Table 5), for the SSC inversion model based on UAV, the calibration R^2 is 0.683, the validation R^2 is 0.707, and the RPD is 2.013. The model has a good fitting degree and high precision. The optimal spectral indexes of SSC were identified as $G \times NIR$, $REG - NIR$, $\sqrt{REG \times G}$, $G + R + REG$, $\sqrt{R \times G}$ and $REG - R$.

In Fig. 4, it can be seen from the scatter diagram of the model that the predicted value of soil salinity is in good agreement with the measured value of soil salinity, and the predicted value and the measured value show a good linear relationship. Therefore, the prediction effect of the SSC model based on UAV is good and has good stability.

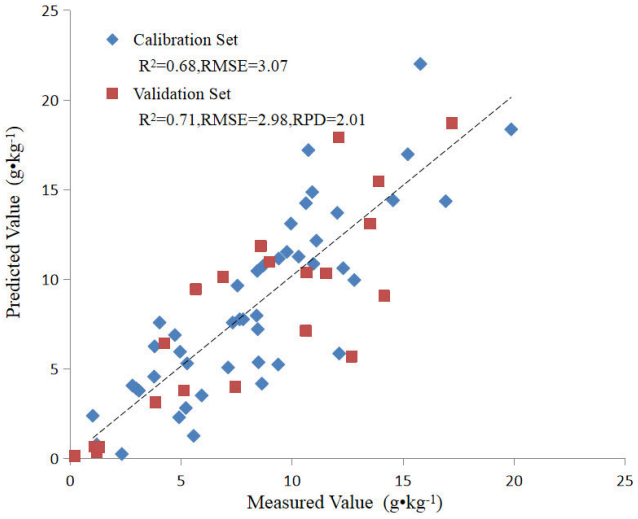

FIGURE 4. Scatter diagram of the best SSC model.

D. FUSION OF SENTINEL-2A-BASED AND UAV-BASED SPECTRAL INDEXES

1) CORRELATION OF SENTINEL-2A-BASED AND UAV-BASED SPECTRAL INDEXES

By comparing the correlations of the Sentinel-2A-based and UAV-based spectral indexes (Table 6), it is concluded that the R between the salt value and spectral indexes based on UAV is significantly higher than that based on Sentinel-2A.

Through the fitting analysis of the spectral index homonymous pixels based on Sentinel-2A and UAV, it is concluded that the fitting degree between the spectral indexes based on Sentinel-2A and UAV is between 0.649 and 0.745 and that there is a certain consistency between the two datasets (Table 7). Therefore, the accuracy of SSC inversion based on Sentinel-2A can be improved by fusing the spectral indexes based on Sentinel-2A and UAV.

2) FUSION OF SENTINEL-2A-BASED SPECTRAL INDEXES BY NUMERICAL REGRESSION

Table 8 shows the fusion parameters converted according to the numerical regression method. Compared with the fused and unfused spectral indexes, the fitting degree of the Sentinel-2A-based spectral indexes is obviously improved.

TABLE 6. Optimal spectral index of UAV and Sentinel-2A imagery and their correlation coefficients with SSC.

No.	Spectral index	Correlation coefficient	
		UAV	Sentinel-2A
1	REG – NIR	0.649*	0. 470*
2	REG – R	0.652*	0.425*
3	G × NIR	-0.666*	-0.511*
4	$\sqrt{REG \times G}$	-0.690*	-0.497*
5	$\sqrt{R \times G}$	-0.699*	-0.497*
6	G + R + REG	-0.695*	-0.480*

Note: * significant correlation at the 0.05 level

TABLE 7. Fitting degree of spectral indexes between UAV and Sentinel-2A.

Spectral index	REG – NIR	REG – R	REG – R	$\sqrt{REG \times G}$	$\sqrt{R \times G}$	G + R + REG
Fitting degree (R^2)	0.649	0.652	0.721	0.715	0.745	0.732

TABLE 8. Spectral index conversion expression and correlation (fused and unfused).

Spectral index	Conversion formula of UAV-based and Sentinel-2A-based spectral index	Fitting degree (R^2)	
		Unfused	Fused
REG – NIR	$S_{REG-NIR}' = 26.003 \times S_{REG-NIR}^2 - 25.73 \times S_{REG-NIR}^2 + 7.0852$	0.649	0.670
REG – R	$S_{REG-R}' = 46.989 \times S_{REG-R}^2 - 38.885 \times S_{REG-R} + 8.777$	0.652	0.678
G × NIR	$S_{G\times NIR}' = 65.922 \times S_{G\times NIR}^2 - 38.837 \times S_{G\times NIR} + 6.238$	0.721	0.784
$\sqrt{REG \times G}$	$S_{\sqrt{REG\times G}}' = 24.751 \times S_{\sqrt{REG\times G}}^2 - 33.974 \times S_{\sqrt{REG\times G}} + 12.74$	0.715	0.766
$\sqrt{R \times G}$	$S_{\sqrt{R\times G}}' = 94.567 \times S_{\sqrt{R\times G}}^2 - 38.856 \times S_{\sqrt{R\times G}} + 4.3572$	0.745	0.792
G + R + REG	$S_{G+R+REG}' = 22.389 \times S_{G+R+REG}^2 - 30.032 \times S_{G+R+REG} + 11.07$	0.732	0.791

TABLE 9. Correlation between Sentinel-2A-based spectral indexes (fused and unfused) and SSC.

Sentinel-2A	Correlation coefficients					
	REG – NIR	REG – R	G × NIR	$\sqrt{REG \times G}$	$\sqrt{R \times G}$	G + R + REG
unfused	0. 470*	0.425*	-0.511*	-0.497*	-0.497*	-0.480*
fused	0.610*	0.607*	-0.626*	-0.625*	-0.629*	-0.621*

Note: * significant correlation at the 0.05 level

Table 9 shows the correlation analysis between the unfused and fused Sentinel-2A-based spectral index and SSC. The correlation coefficients between the fused spectral indexes and SSC were improved by 0.115-0.182.

E. SPATIAL DISTRIBUTION OF REGIONAL SSC

1) SPATIAL DISTRIBUTION OF SSC INVERTED BASED ON UAV IN THE TEST AREA

Fig. 5 shows the SSC inversion map of the test area constructed on April 26, 2018, based on the UAV-based SSC inversion model. The inversion value of SSC in the test area is 0.204-20.871 $g \cdot kg^{-1}$, and the average salt value is 8.348 $g \cdot kg^{-1}$. In the 85 samples, the observed values of 73 samples were coherent in comparison with the ground truth data, accounting for 85.88% of the total, which indicated that most of the inversion results were similar to the ground truth results. Therefore, the SSC model based on UAV data employing the MSLR method can achieve good SSC inversion results. A statistical analysis of the data was performed, and the classification results of each level are shown in Table 10.

In Table 10, it can be seen that the area with moderately and severely saline soil in the test area is large, accounting for 75.273% of the total. Soil salinization in this area is relatively common, with most of the region having severely saline soil. The inversion results are similar to the field survey results.

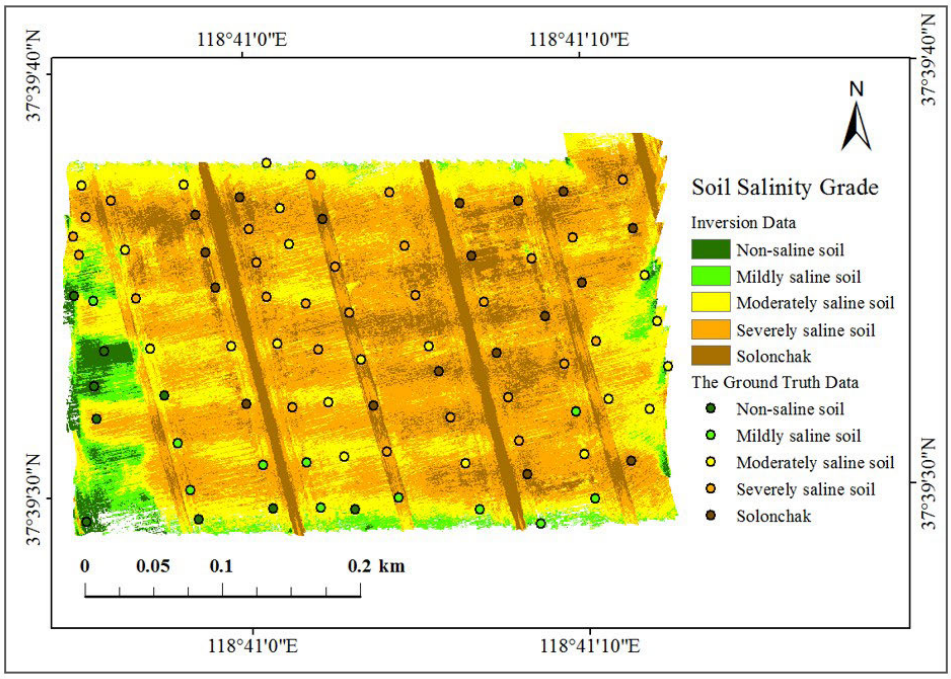

FIGURE 5. Soil salinity grade map of the test area in spring 2018.

TABLE 10. Soil salinity grades and their percentages in the study area.

Grade	Inversion map	
	Pixel elements	Percentage (%)
Non-saline soil (<2.0 g·kg^{-1})	2,605,396	6.29
Mildly saline soil (≥ 2.0-4.0 g·kg^{-1})	3,523,841	8.51
Moderately saline soil (≥ 4.0-6.0 g·kg^{-1})	12,005,401	28.98
Severely saline soil (≥ 6.0-10.0 g·kg^{-1})	19,289,990	46.57
Solonchak (≥ 10.0 g·kg^{-1})	3,995,963	9.65

2) SSC INVERSION MODEL AND SPATIAL DISTRIBUTION IN THE STUDY AREA

Table 11 compares scenario 1, scenario 2, and scenario 3. The accuracy of scenario 3 was significantly higher than that of the other two scenarios. The calibration R^2 was improved by 0.09-0.14, the calibration RMSE was reduced by 0.55-0.75, the validation R^2 was improved by 0.09-0.10, the validation RMSE was reduced by 0.56-0.74, and the RPD was improved by 0.32-0.37. Thus, the numerical regression method can improve the remote sensing inversion accuracy of SSC satellite.

Fig. 6 shows the SSC inversion map using the UAV-based SSC inversion model and fused Sentinel-2A imagery, and Table 12 shows the relevant data statistics.

The following observations can be made from Fig. 6 and Table 12: (1) The SSC in the study area is high in the southwest and low in the northeast, which is similar to the high terrain in the southwest and low terrain in the northeast in this area. This is consistent with previous research showing that the degree of soil salinization gradually increases with the terrain from high to low and from upstream to downstream [33], [44]. (2) The salt value increases from the inland to coastal areas. This conclusion is consistent with the fact that the groundwater level is low and the hydrodynamic forcing between the fresh water and sea water has been destroyed, which causes the sea water to rapidly infiltrate the land. (3) In the study area, the percentage of solonchak saline soil is the largest among all salinity levels, with a value of 30.17%, whereas the percentage of non-saline soil is the lowest, with a value of 8.55%. It can be seen that the phenomenon of soil salinization is relatively common and severe across the whole study area. The inversion results are consistent with the actual conditions in the study area, which indicates that the model is effective for the accurate inversion of SSC satellite remote sensing data.

V. DISCUSSION

1) In this study, samples were collected in spring. The characteristics of low precipitation and vegetation coverage in this season cause the soil spectrum to show a good response to SSC, which is consistent with the study by Zhang *et al.* [37], in which spring was

TABLE 11. Spectral index fusion expression and correlation (fused and unfused).

Scenario	Model	Sentinel-2A image	Formula	Calibration		Validation		
				R^2	RMSE	R^2	RMSE	RPD
Scenario 1	Based on Sentinel-2A model	Spectral index (unfused)	$Y = -49.449 - 698.176 \times R \times REG + 149.077 \times (R + NIR) + 148.392 \times \sqrt{R^2 + G^2} - 2569.093 \times G \times R \times REG + 228.649 \times G \times REG$	0.49	4.62	0. 49	4.54	1.44
Scenario 2	Based on UAV model	Spectral index (unfused)	$Y = 58.856 + 166.915 \times G \times NIR + 87.456 \times (REG - NIR) - 1273.268 \times \sqrt{REG \times G} + 197.594 \times (G + R + REG) + 505.55 \times \sqrt{R \times G} + 479.896 \times (REG - R)$	0.57	4.28	0.50	4.02	1.63
Scenario 3		Spectral index (fused)	$Y = 58.856 + 166.915 \times G \times NIR + 87.456 \times (REG - NIR) - 1273.268 \times \sqrt{REG \times G} + 197.594 \times (G + R + REG) + 505.55 \times \sqrt{R \times G} + 479.896 \times (REG - R)$	0.60	3.57	0.56	3.51	1.87

TABLE 12. Soil salinity grades and their percentages in the study area.

Grade	Pixel elements	Percentage (%)
Non-saline soil (<2.0 g·kg^{-1})	288,955,007	8.55
Mildly saline soil (≥ 2.0-4.0 g·kg^{-1})	340,108,022	10.07
Moderately saline soil (≥ 4.0-6.0 g·kg^{-1})	828,313,407	24.52
Severely saline soil (≥ 6.0-10.0 g·kg^{-1})	901,692,310	26.69
Solonchak (≥ 10.0 g·kg^{-1})	1,019,456,422	30.17

the sampling time associated with the inversion of SSC and good inversion results were obtained. The model obtained in this study has good SSC prediction results in this season, but whether the same result can be obtained in other seasons remains to be studied.

2) This study shows that the response effect of SSC spectra based on UAV was significantly better than that based on Sentinel-2A. Because the spatial resolution of UAV images is much higher than that of Sentinel-2A images, the actual ground area covered by a single pixel based on UAV is smaller, and the identification of SSCs by UAV is more accurate [45]–[47]. This is generally consistent with the result that the SSC spectral response based on UAV was significantly better than that based on the satellite, which was also found by Chen *et al.* [48] using UAV and GF-1 satellites to retrieve soil salt data in the sand-trench irrigation area of the Hetao irrigation area.

3) In this study, UAV and Sentinel-2A images with different spatial resolutions at the same time scale were used. By analyzing the internal relationship between the spectral indexes based on UAV and Sentinel-2A, a numerical regression method was introduced to fit the quadratic polynomials between the spectral indexes based on these two methods to improve the accuracy of SSC inversion based on Sentinel-2A and provide a new idea for realizing the fusion of multisource remote sensing images at the spatial scale. Some scholars have used similar methods to fuse satellite remote sensing images of different time scales. For example, Chen *et al.* [49] used the numerical regression method to fit four Landsat TM5, OLI and ALI images obtained in April over four years, 2000-2016, realizing the fusion of SSC information in the Yellow River Delta considering a temporal scale. It is confirmed that the fusion of different spectral data with the numerical regression method is effective for SSC monitoring.

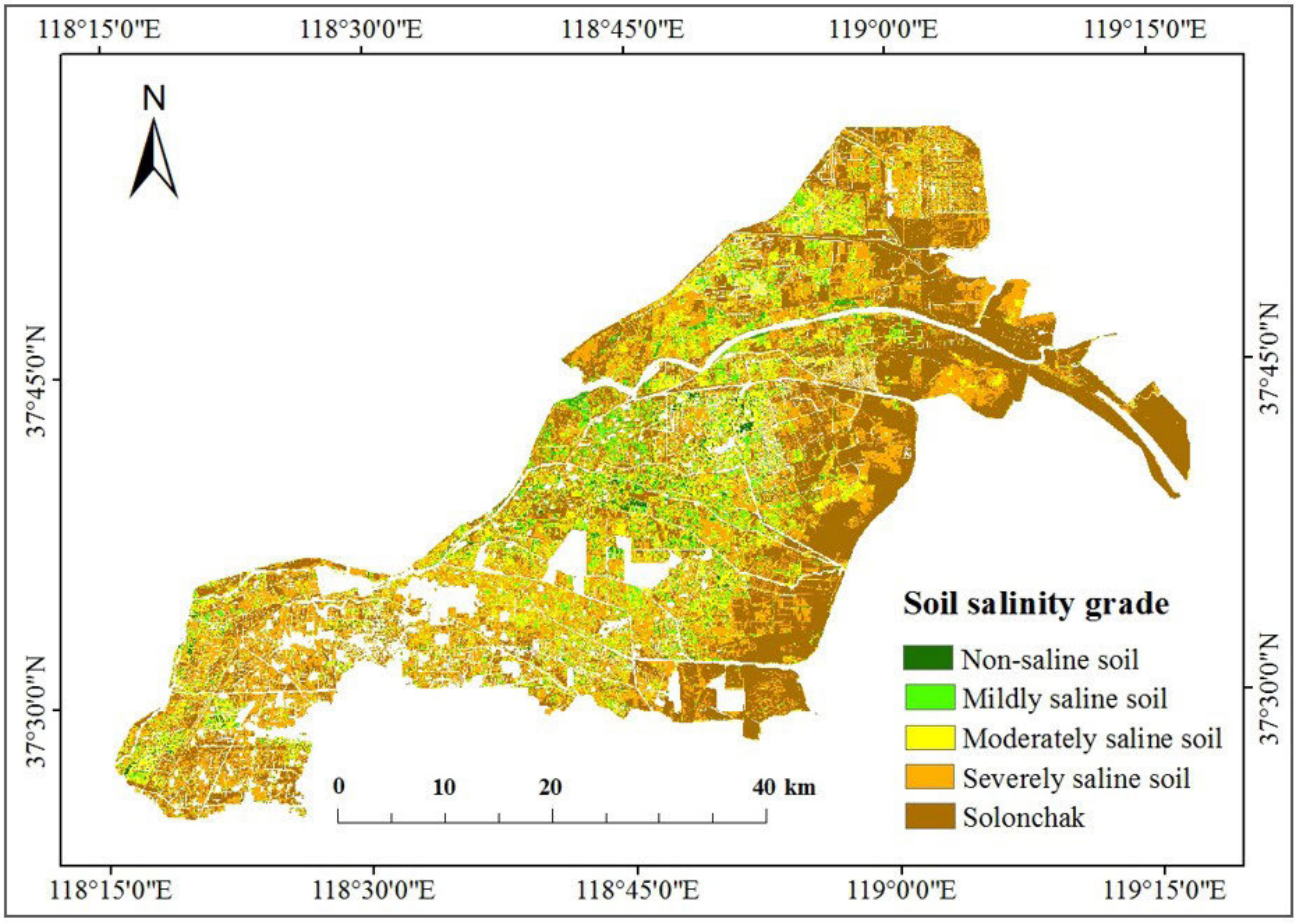

FIGURE 6. The SSC inversion map using the UAV-based SSC inversion model and fused Sentinel-2A imagery.

4) The remote sensing monitoring of soil salinization is easily affected by soil texture, soil moisture, etc. In the study area, the soil texture is mainly loam and relatively uniform; thus, the effect of soil texture could not be considered. In the sampling period (April 26, 2018), the precipitation in the study area was low, and the soil surface was relatively dry. The soil samples were collected from the topsoil (0-5 cm); thus, the influence of soil moisture on soil salinization monitoring is lighter. For other seasons and different regions, removing of the influence of soil moisture and texture may be important considerations in future studies. Partial correlation analysis could be helpful for the removing of the influence of soil moisture [50].

VI. CONCLUSION

In this paper, based on UAV and Sentinel-2A images, the Sentinel-2A-based and UAV-based spectral indexes of SSC were fused with a numerical regression method to correct the SSC spectral indexes based on Sentinel-2A, and the SSC inversion model based on the UAV-based spectral indexes was applied to the corresponding data of the fused Sentinel-2A images for the SSC inversion in the study area. The following conclusions were reached:

1) Based on MSLR, the six following optimal spectral indexes of SSC were identified: $G \times NIR$, $REG - NIR$, $\sqrt{REG \times G}$, $G + R + REG$, $\sqrt{R \times G}$ and $REG - R$. A SSC inversion model based on UAV spectral indexes was constructed, with a calibration R^2 of 0.683, a validation R^2 of 0.707, and an RPD of 2.013, which showed that the model accuracy was high and stable.
2) By verifying the application of the UAV-based SSC inversion model to the Sentinel-2A image, it was concluded that when the model was applied to the fused Sentinel-2A imagery, its calibration R^2 was improved by 0.078-0.111, the calibration RMSE was decreased by 0.338-1.048, the validation R^2 was improved by 0.019-0.079, the validation RMSE was decreased by 0.517-1.030, and the RPD was improved by 0.185-0.423. This result indicates that this method can improve the accuracy of SSC remote sensing inversion. It is proven that the numerical regression method used to fuse spectral indexes based on Sentinel-2A and UAV can improve the accuracy of regional SSC inversion.
3) Based on the inversion of the fused SSC spectral index based on Sentinel-2A and UAV, the overall distribution trend of SSC in the study area was low in the southwest and high in the northeast. The solonchak percentage was 30.17%, the moderately and severely saline soil covered 51.21%, and the phenomenon of soil salinization was relatively common

and severe, which was consistent with the actual conditions. Therefore, the fusion of SSC spectral indexes based on Sentinel-2A and UAV according to the numerical regression method can improve the accuracy of SSC satellite remote sensing inversion, which is conducive to the accurate and rapid monitoring of SSC.

ACKNOWLEDGMENT

The author would like to thank the referees and the editor for their valuable comments and efforts in reviewing and handling their article. They would also like to thank the ESA for the Sentinel-2A data. They would also like to thank the financial support for this study.

REFERENCES

[1] H. Chen, G. Zhao, Y. Li, D. Wang, and Y. Ma, "Monitoring the seasonal dynamics of soil salinization in the Yellow River Delta of China using Landsat data," *Natural Hazards Earth Syst. Sci.*, vol. 19, no. 7, pp. 1499–1508, Jul. 2019.

[2] Y. Liu, X.-Z. Pan, R.-J. Shi, Y.-L. Li, C.-K. Wang, and Z.-T. Li, "Predicting soil salt content over partially vegetated surfaces using non-negative matrix factorization," *IEEE J. Sel. Topics Appl. Earth Observ. Remote Sens.*, vol. 8, no. 11, pp. 5305–5316, Nov. 2015.

[3] A. Sidike, S. Zhao, and Y. Wen, "Estimating soil salinity in Pingluo County of China using QuickBird data and soil reflectance spectra," *Int. J. Appl. Earth Observ. Geoinf.*, vol. 26, pp. 156–175, Feb. 2014.

[4] E. Scudiero, T. H. Skaggs, and D. L. Corwin, "Comparative regional-scale soil salinity assessment with near-ground apparent electrical conductivity and remote sensing canopy reflectance," *Ecol. Indicators*, vol. 70, pp. 276–284, Nov. 2016.

[5] J. Chen, S. Wan, H. Liu, S. Fan, Y. Zhang, W. Wang, M. Xia, R. Yuan, F. Deng, and F. Shen, "Overexpression of an apocynum venetum DEAD-box helicase gene (AvDH1) in cotton confers salinity tolerance and increases yield in a saline field," *Frontiers Plant Sci.*, vol. 6, p. 1227, Jan. 2016.

[6] H.-S. Wang, C. Yu, X.-F. Tang, Z.-J. Zhu, N.-N. Ma, and Q.-W. Meng, "A tomato endoplasmic reticulum (ER)-type omega-3 fatty acid desaturase (LeFAD3) functions in early seedling tolerance to salinity stress," *Plant Cell Rep.*, vol. 33, no. 1, pp. 131–142, Jan. 2014.

[7] K. Yan, M. Cui, S. Zhao, X. Chen, and X. Tang, "Salinity stress is beneficial to the accumulation of chlorogenic acids in honeysuckle (Lonicera japonica Thunb.)," *Frontiers Plant Sci.*, vol. 7, p. 1563, Oct. 2016.

[8] Y. Guo, Z. Shi, L.-Q. Zhou, X. Jin, Y.-F. Tian, and H.-F. Teng, "Integrating remote sensing and proximal sensors for the detection of soil moisture and salinity variability in coastal areas," *J. Integrative Agricult.*, vol. 12, no. 4, pp. 723–731, Apr. 2013.

[9] C. Zhao, "Research and application progress of agricultural remote sensing," *Trans. Chin. Soc. Agricult. Mach.*, vol. 45, no. 12, pp. 277–293, Dec. 2014.

[10] H. Su, B. Yong, and Q. Du, "Hyperspectral band selection using improved firefly algorithm," *IEEE Geosci. Remote Sens. Lett.*, vol. 13, no. 1, pp. 68–72, Jan. 2016.

[11] F. Yu, E. Song, H. Liu, J. Zhu, and C.-C. Hung, "Laparoscopic image-guided system based on multispectral imaging for the ureter detection," *IEEE Access*, vol. 7, pp. 3800–3809, Dec. 2019.

[12] J. Ma, W. Sun, G. Yang, and D. Zhang, "Hydrological analysis using satellite remote sensing big data and CREST model," *IEEE Access*, vol. 6, pp. 9006–9016, Feb. 2018.

[13] H. Su, B. Zhao, Q. Du, and P. Du, "Kernel collaborative representation with local correlation features for hyperspectral image classification," *IEEE Trans. Geosci. Remote Sens.*, vol. 57, no. 2, pp. 1230–1241, Feb. 2019.

[14] J. Martínez, G. Egea, J. Agüera, and M. Pérez-Ruiz, "A cost-effective canopy temperature measurement system for precision agriculture: A case study on sugar beet," *Precis. Agricult.*, vol. 18, no. 1, pp. 95–110, Feb. 2017.

[15] L. Hassan-Esfahani, A. Torres-Rua, A. Jensen, and M. McKee, "Assessment of surface soil moisture using high-resolution multi-spectral imagery and artificial neural networks," *Remote Sens.*, vol. 7, no. 3, pp. 2627–2646, Mar. 2015.

[16] C. Zhang, "The application of small unmanned aerial systems for precision agriculture: A review," *Precis. Agricult.*, vol. 13, no. 6, pp. 693–712, Dec. 2012.

[17] H. Hoffmann, R. Jensen, A. Thomsen, H. Nieto, J. Rasmussen, and T. Friborg, "Crop water stress maps for an entire growing season from visible and thermal UAV imagery," *Biogeosciences*, vol. 13, no. 24, pp. 6545–6563, Aug. 2016.

[18] H. Zhang, C. Cao, L. Xu, and T. A. Gulliver, "A UAV detection algorithm based on an artificial neural network," *IEEE Access*, vol. 6, pp. 24720–24728, May 2018.

[19] Q. Liu, T. Zhang, Y. Li, Y. Li, C. Bu, and Q. Zhang, "Comparative analysis of fractional vegetation cover estimation based on multi-sensor data in a semi-arid sandy area," *Chin. Geographical Sci.*, vol. 29, no. 1, pp. 166–180, Feb. 2019.

[20] D. An, G. Zhao, C. Chang, Z. Wang, P. Li, T. Zhang, and J. Jia, "Hyperspectral field estimation and remote-sensing inversion of salt content in coastal saline soils of the Yellow River Delta," *Int. J. Remote Sens.*, vol. 37, no. 2, pp. 455–470, Jan. 2016.

[21] C. Pohl and J. L. Van Genderen, "Review article multisensor image fusion in remote sensing: Concepts, methods and applications," *Int. J. Remote Sens.*, vol. 19, no. 5, pp. 823–854, Mar. 1998.

[22] Y. Chen, C. Li, P. Ghamisi, X. Jia, and Y. Gu, "Deep fusion of remote sensing data for accurate classification," *IEEE Geosci. Remote Sens. Lett.*, vol. 14, no. 8, pp. 1–5, Jun. 2017.

[23] Y. Yang, W. Wan, S. Huang, F. Yuan, S. Yang, and Y. Que, "Remote sensing image fusion based on adaptive IHS and multiscale guided filter," *IEEE Access*, vol. 4, pp. 4573–4582, Sep. 2016.

[24] A. Azarang, H. E. Manoochehri, and N. Kehtarnavaz, "Convolutional autoencoder-based multispectral image fusion," *IEEE Access*, vol. 7, pp. 35673–35683, Mar. 2019.

[25] J. Guo, Z. Xie, Y. Qin, L. Jia, and Y. Wang "Short-term abnormal passenger flow prediction based on the fusion of SVR and LSTM," *IEEE Access*, vol. 7, pp. 42946–42955, Mar. 2019.

[26] I. Nurmemet, A. Ghulam, T. Tiyip, R. Elkadiri, J.-L. Ding, M. Maimaitiyiming, A. Abliz, M. Sawut, F. Zhang, A. Abliz, and Q. Sun, "Monitoring soil salinization in Keriya River Basin, Northwestern China using passive reflective and active microwave remote sensing data," *Remote Sens.*, vol. 7, no. 7, pp. 8803–8829, Jul. 2015.

[27] A. Kerim, T. Tiyip, and D. Zhang, "Calibration and validation of soil salt model based on hyperspectral ASTER image," *Trans. Chin. Soc. Agricult. Eng.*, vol. 32, no. 12, pp. 144–150, Jun. 2016.

[28] C. He, B. Gao, Q. Huang, Q. Ma, and Y. Dou, "Environmental degradation in the urban areas of China: Evidence from multi-source remote sensing data," *Remote Sens. Environ.*, vol. 193, pp. 65–75, May 2017.

[29] P. Li, G. Zhao, M. Gao, C. Chang, and Z. Wang, "Hyperspectral estimation and remote sensing inversion of soil water content in the Yellow River Delta," *Acta Pedologica Sinica*, vol. 52, no. 6, pp. 1262–1272, May 2015.

[30] H. Wu, X. Han, and H. Yang, "Exploration and research on the development of efficient eco agriculture in the Yellow River Delta, taking Dongying City as an example," *Technol. Econ. Guide*, no. 25, pp. 116–118, Sep. 2017.

[31] W. Su, M. Zhang, K. Jang, D. Zhu, J. Hang, and P. Wang, "Atmospheric correction method for Sentinel-2 satellite imagery," *Acta Optica Sinica*, vol. 38, no. 1, pp. 314–323, Jan. 2018.

[32] L. Bai, C. Wang, S. Zang, Y. Zhang, Q. Hao, and Y. Wu, "Remote sensing of soil alkalinity and salinity in the Wuyu'er–Shuangyang River Basin, Northeast China," *Remote Sens.*, vol. 8, no. 2, p. 163, Feb. 2016.

[33] Z. Gao, X. Xu, J. Wang, H. Yang, W. Huang, and H. Feng, "A method of estimating soil moisture based on the linear decomposition of mixture pixels," *Math. Comput. Model.*, vol. 58, nos. 3–4, pp. 606–613, Aug. 2013.

[34] A. E. K. Douaoui, H. Nicolas, and C. Walter, "Detecting salinity hazards within a semiarid context by means of combining soil and remote-sensing data," *Geoderma*, vol. 134, nos. 1–2, pp. 217–230, Sep. 2006.

[35] C. J. Tucker, "Red and photographic infrared linear combinations for monitoring vegetation," *Remote Sens. Environ.*, vol. 8, no. 2, pp. 127–150, May 1979.

[36] H. Triki Fourati, M. Bouaziz, M. Benzina, and S. Bouaziz, "Modeling of soil salinity within a semi-arid region using spectral analysis," *Arabian J. Geosci.*, vol. 8, no. 12, pp. 11175–11182, Dec. 2015.

[37] S. Zhang and G. Zhao, "A harmonious satellite-unmanned aerial vehicle-ground measurement inversion method for monitoring salinity in coastal saline soil," *Remote Sens.*, vol. 11, no. 14, p. 1700, Jul. 2019.

[38] J. Wang, J. Ding, D. Yu, X. Ma, Z. Zhang, X. Ge, D. Teng, X. Li, J. Liang, I. Lizaga, X. Chen, L. Yuan, and Y. Guo, "Capability of Sentinel-2 MSI data for monitoring and mapping of soil salinity in dry and wet seasons in the Ebinur Lake Region, Xinjiang, China," *Geoderma*, vol. 353, pp. 172–187, Nov. 2019.
[39] Y. Hong, R. Shen, H. Cheng, S. Chen, Y. Chen, L. Guo, J. He, Y. Liu, L. Yu, and Y. Liu, "Cadmium concentration estimation in peri-urban agricultural soils: Using reflectance spectroscopy, soil auxiliary information, or a combination of both?" *Geoderma*, vol. 354, Nov. 2019, Art. no. 113875.
[40] T. Zhang, G. Zhao, and M. Gao, "Salt estimation and remote sensing inversion of winter wheat planting area in the Yellow River Delta Based on near earth multispectral and oli images, taking Kenli County and Wudi County of Shandong Province as examples," *J. Natural Resour.*, vol. 31, no. 6, pp. 1051–1060, 2016.
[41] S. Nawar, H. Buddenbaum, and J. Hill, "Digital mapping of soil properties using multivariate statistical analysis and ASTER data in an arid region," *Remote Sens.*, vol. 7, no. 2, pp. 1181–1205, Jan. 2015.
[42] T. Miura, A. Huete, and H. Yoshioka, "An empirical investigation of cross-sensor relationships of NDVI and red/near-infrared reflectance using EO-1 hyperion data," *Remote Sens. Environ.*, vol. 100, no. 2, pp. 223–236, Jan. 2006.
[43] H. Chen, G. Zhao, J. Chen, R. Wang, and M. Gao, "Remote sensing inversion of salt content in the Yellow River Estuary based on improved vegetation index," *Trans. Chin. Soc. Agricult. Eng.*, vol. 3, no. 5, pp. 107–114, Mar. 2015.
[44] G. Metternicht and J. A. Zinck, "Spatial discrimination of salt-and sodium-affected soil surfaces," *Int. J. Remote Sens.*, vol. 18, no. 12, pp. 2571–2586, Aug. 1997.
[45] X. Huang and L. Zhang, "An SVM ensemble approach combining spectral, structural, and semantic features for the classification of high-resolution remotely sensed imagery," *IEEE Trans. Geosci. Remote Sens.*, vol. 51, no. 1, pp. 257–272, Jan. 2013.
[46] H. Shakhatreh, A. H. Sawalmeh, A. Al-Fuqaha, Z. Dou, E. Almaita, I. Khalil, N. S. Othman, A. Khreishah, M. Guizani, "Unmanned aerial vehicles (UAVs): A survey on civil applications and key research challenges," *IEEE Access*, vol. 7, pp. 48572–48634, Apr. 2018.
[47] F. Paul, N. E. Barrand, S. Baumann, E. Berthier, and T. Bolch, "On the accuracy of glacier outlines derived from remote-sensing data," *Ann. Glaciol.*, vol. 54, no. 63, pp. 171–182, Jul.2013.
[48] J. Chen, X. Wang, Z. Zhang, J. Han, Z. Yao, and G. Wei, "Soil salinization monitoring method based on UAV and satellite remote sensing," *Trans. Chin. Soc. Mach.*, vol. 50, no. 12, pp. 161–169, Dec. 2019.
[49] W. Chen, Y. Weng, X. Fan, and Y. Cao, "Soil salt inversion and dynamic analysis based on spectral transformation," *J. Southeast Univ. Natural Sci. Ed.*, vol. 47, no. 6, pp. 1233–1238, Nov. 2017.
[50] H. Cheng, R. Shen, Y. Chen, Q. Wan, T. Shi, J. Wang, Y. Wan, Y. Hong, and X. Li, "Estimating heavy metal concentrations in suburban soils with reflectance spectroscopy," *Geoderma*, vol. 336, pp. 59–67, Feb. 2019.

YING MA received the B.S. degree in land resource management from Shandong Agricultural University, Tai'an, China, in 2019, where she is currently pursuing the M.S. degree in land resource management. Her research interests include soil quantitative remote sensing and multisource remote sensing fusion.

HONGYAN CHEN received the B.S. degree in land resources management, the M.S. in pedology, and the Ph.D. degree in land resources utilization from Shandong Agricultural University, in 2001, 2004, and 2012, respectively. From 2013 to 2016, she was a Postdoctoral Research Fellow of agricultural engineering with Shandong Agricultural University. She is currently an Associate Professor with the College of Resources and Environment, Shandong Agricultural University. Her research interests include soil quantitative remote sensing and information technology.

GENGXING ZHAO received the B.S. degree in pedology from Shandong Agricultural University, in 1985, and the M.S. and Ph.D. degrees in pedology from Zhejiang University, in 1990 and 1997, respectively. He is currently a Professor with the College of Resources and Environment, Shandong Agricultural University. His research interests include land resources, remote sensing, and information technology application. He is the Director of the China Land Society, the Deputy Director of the Remote Sensing and Information Professional Committee of China Soil Society, the Director of the Shandong Soil Fertilizer Society, the Director of the Shandong Land Society, and a member of the Shandong Agricultural Expert Advisory Group.

ZHUORAN WANG received the B.S. degree in land resource management from Shandong Jianzhu University, in 2012, and the M.S. and Ph.D. degrees in pedology from Shandong Agricultural University, in 2017. Since 2017, he has been a Lecturer with the College of Resources and Environment, Shandong Agricultural University. His research interests include land evaluation and information technology.

DANYANG WANG received the B.S. degree in land resource management and the M.S. degree in agricultural engineering and information technology from Shandong Agricultural University, in 2018 and 2020, respectively. Her research interest includes soil quantitative remote sensing.